

Insights into Phase Evolution and Mechanical Behavior of the Eutectoid Ti–6.4(wt%)Ni Alloy Modified with Fe and Cr

Verena Pfaffinger, Ella Staufer, Christian Edtmaier, Aurel Arnoldt, Martin Schmitz-Niederer, Jelena Horky, and Thomas Klein*

Titanium alloys gain increasing importance in industry due to the expansion of advanced manufacturing technologies such as additive manufacturing. Conventional titanium alloys processed by such technologies suffer from formation of large primary grains and anisotropy of mechanical properties. Therefore, novel alloys are required. Herein, the effect of ternary alloying elements Fe and Cr on the Ti–6.4(wt%)Ni eutectoid system is investigated. Both elements act as eutectoid formers. Fe and Cr show sluggish transformation behavior, whereas Ni is an active eutectoid-forming element. Thereby, sluggish refers to slow and active to fast transformation kinetics. The focus of this work is on the combined addition of such elements studied under different heat-treatment conditions. It is shown in the results that largely varying microstructures can be generated resulting in hardness values ranging from 239 to 556 HV_{0.1}. Moreover, the formation of a substructure within the α phase of direct aged alloys is observed. The formation mechanism of this substructure is investigated in detail. The mechanical properties are discussed based on the microstructural characteristics. The presence of intermetallic Ti₂Ni phase increases the Young's modulus, whereas the presence of ω phase results in embrittlement. The results shed light upon the complex phase formation and decomposition behavior of titanium alloys based on Ti–6.4Ni.

1. Introduction

Titanium alloys have received considerable attention from industry and academia due to their high specific strength, next to other beneficial properties such as high modulus and strength retention at elevated temperatures as well as good oxidation and corrosion resistance.^[1] Based on their property portfolio, they are in use for space and aviation structures, biomedical applications, and chemical industries, among other demanding fields of application. Various processing techniques have been explored for the fabrication of complex structures but recently, most attention has shifted to additive manufacturing (AM). AM of metal alloys can provide substantial economic and ecological benefits because material waste is dramatically reduced during the fabrication of various components.^[2] Moreover, added value can be generated by increased design freedom and integration of additional functionalities.^[3] For large-scale structures, in particular, directed energy deposition processes using


wire feedstock such as wire-arc directed energy deposition (waDED), are of interest.^[4–6] Thereby, metal wires are melted by an electric or plasma arc and consecutively deposited along a predefined path.^[7–10] The interest in AM and waDED of titanium is particularly high as the economic benefits are most obvious due to the high cost and ecological impact of its primary production.^[1] Approximately 50% of the total product costs of conventionally fabricated titanium structures are required for machining operations,^[11] whereby, in many instances, 80% of scrap is generated in the form of offcuts and chippings.^[12] Conventional alloys (Ti–6Al–4V or similar) are, however, not optimized for waDED processes resulting in a textured and coarse microstructure and anisotropic mechanical properties.^[13–15] This suboptimal microstructure is due to the epitaxial nucleation of new grains at preexisting grains of the prior layer and preferential growth along the pronounced thermal gradient. Recently, several works explored the introduction of transition metals into titanium alloys.^[16–23] Zhang et al.^[16] suggested that alloying elements with pronounced partitioning behavior into the remaining melt during solidification and a steep liquidus curve provide a high growth restriction factor, resulting in grain refinement and a strong reduction of texture

V. Pfaffinger, A. Arnoldt, T. Klein
LKR Light Metals Technologies
Austrian Institute of Technology
5282 Ranshofen, Austria
E-mail: thomas.klein@ait.ac.at

E. Staufer, C. Edtmaier
Institute of Chemical Technologies and Analytics
TU Wien
1060 Vienna, Austria

M. Schmitz-Niederer
voestalpine Böhler Welding Germany GmbH
59067 Hamm, Germany

J. Horky
RHP-Technology GmbH
2444 Seibersdorf, Austria

 The ORCID identification number(s) for the author(s) of this article can be found under <https://doi.org/10.1002/adem.202300177>.

© 2023 The Authors. Advanced Engineering Materials published by Wiley-VCH GmbH. This is an open access article under the terms of the Creative Commons Attribution-NonCommercial License, which permits use, distribution and reproduction in any medium, provided the original work is properly cited and is not used for commercial purposes.

DOI: 10.1002/adem.202300177

and anisotropy. Zhang et al.^[16] used Cu additions, but similar effects have been demonstrated using Fe,^[17–20] Ni,^[19,21,22] and Co.^[23]

The transition metals mentioned before belong to the group of β -eutectoid-forming elements when added to Ti.^[1,24] Upon heat treatment below the eutectoid temperature, the β -phase decomposes into α phase and various intermetallic phases with different stoichiometry and crystallography. Depending on the kinetics of this reaction, these alloys have historically been classified into active eutectoids (Cu, Ni, Zn, Si) and sluggish eutectoids (Fe, Cr, Mn, Co among others).^[25,26] In this context, active refers to fast reaction kinetics that occur even during rapid cooling, and sluggish refers to slow reaction kinetics that can easily be suppressed and only occur during long-term aging. The formed reaction products may either form pearlite-like structures or more complex aggregates, sometimes referred to as bainite, depending on the cooling rate or, more general, on the heat-treatment procedure.^[24] As a result of the created microstructure, varying effects on the mechanical properties are observed. Due to the potential for grain refinement upon solidification^[19,21] and the option to form intermetallic phases (in reasonable times, that is, by using an active eutectoid-forming element),^[26] Ni was chosen as major alloying element in the present study.

Additionally, this work explores the effects of ternary additions of the sluggish eutectoid-forming elements Fe and Cr on the Ti–6.4(wt%)Ni base system with the aim of modifying the transition sequence and the mechanical properties. These alloy systems are microstructurally investigated after different heat treatments using scanning electron microscopy (SEM) including electron back-scatter diffraction (EBSD) and X-ray diffraction (XRD), and by thermodynamic calculations. The mechanical characteristics are determined by microhardness testing, compression testing, and ultrasonic-based Young’s modulus determination. The combination of these techniques gives insights into phase-transformation phenomena and resultant material properties and contributes to the understanding of ternary alloying element additions on the Ti–Ni alloy system.

2. Results and Discussion

2.1. Thermodynamic Calculations

The phase fraction diagrams of the investigated alloys are depicted in **Figure 1** with a) Ti–6.4Ni, b) Ti–6.4Ni–2Fe, and

c) Ti–6.4Ni–2Cr. All alloy compositions are given in weight percent (wt%) throughout this paper. All three alloys show complete solidification via the β phase. The eutectoid temperature of the binary alloy is ≈ 767 °C and is shifted to ≈ 748 °C by introduction of Fe and to ≈ 742 °C by introduction of Cr. The reduction of the eutectoid temperature with addition of Fe or Cr underpins their β -stabilizing effect. The addition of both Fe and Cr shift the alloy composition from eutectoid to slightly hypereutectoid. In case of the binary- as well as the Fe-modified alloy, complete transformation to α phase and Ti_2Ni phase is predicted.^[21,22,26] In case of the Cr-modified alloy variant, the introduction of an ordered variant of the β phase (β_o) is suggested by thermodynamic calculation, which is in agreement with ref. [27].

2.2. Microstructure and Hardness Evolution upon Heat Treatment

Microstructural and mechanical property characterization was performed using specimens manufactured by arc-based button melting. This technique establishes cooling rates that are of equivalent magnitude as in typical waDED processes.^[28,29] However, it cannot mirror the effects of the repetitive reheating (intrinsic heat treatment) occurring during waDED.^[30] **Figure 2** gives an overview of all microstructural conditions investigated. The micrographs of **Figure 2a–c** correspond to the heat-treatment condition 1, that is, solution heat-treated and quenched. In all materials, lath-like features corresponding to the α phase are discernible. These laths show the finest dimensions and highest aspect ratio in the binary alloy variant. In **Figure 2c**, corresponding to the Ti–6.4Ni–2Cr alloy, the α -phase laths are substantially broader than in the other alloys. In all three alloys, bright phases are visible between the α -phase laths corresponding to the β phase. The strong contrast is a result of the enrichment of the heavy elements Ni, Fe, and Cr, which typically diffuse toward α -lath boundaries during the phase transformation, thereby, stabilizing β -phase films in these regions.

The hardness values of each alloy and condition are shown alongside the microstructural images. In the quenched material condition, the highest hardness is observed in the binary Ti–6.4Ni alloy. Both ternary alloys show reduced hardness, which qualitatively corresponds to the dimension of the α -phase laths and may, thus, be explained by a Hall–Petch effect.^[31]

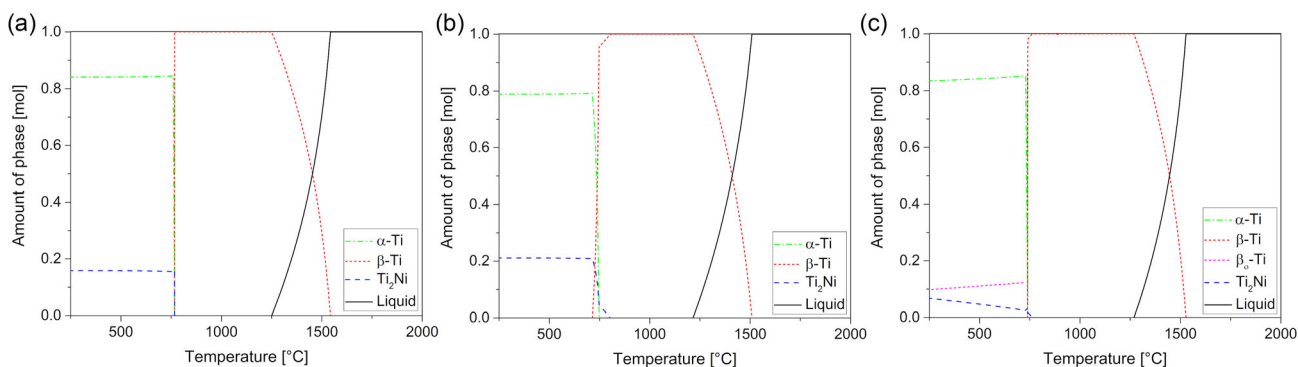


Figure 1. Phase fraction diagrams calculated using Thermo–Calc for a) Ti–6.4Ni; b) Ti–6.4Ni–2Fe, and c) Ti–6.4Ni–2Cr.

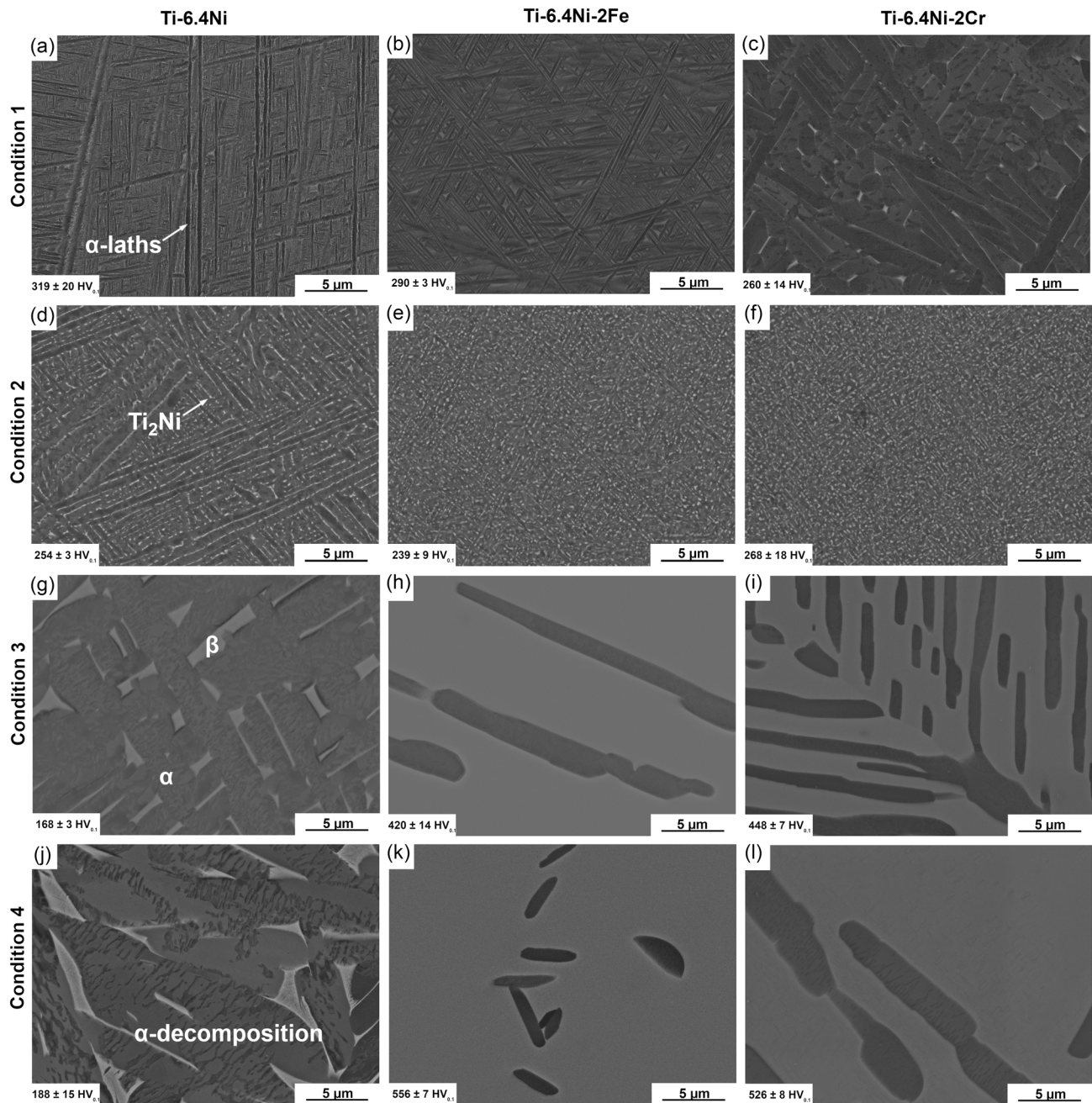


Figure 2. Scanning electron microscopy (SEM) images taken in backscattered electron mode (15 kV, 4Q-BSE detector); a–c) condition 1 (quenched from 900 °C); d–f) condition 2 (quenched from 900 °C and aged at 600 °C for 1 h); g–i) condition 3 (quenched from 900 to 730 °C and aged for 1 h); and j–l) condition 4 (quenched from 900 °C and direct aged at 770 °C). Images of the left column were taken from the binary Ti–6.4Ni alloy, center column images from the ternary Ti–6.4Ni–2Fe alloy and the images from the right column were taken from the ternary Ti–6.4Ni–2Cr alloy.

Figure 2d–f visualizes the resultant microstructure after the solution heat treatment and subsequent aging at 600 °C for 1 h (condition 2). In the binary alloy (Figure 2d), the lath-like structure is remanent. However, the inter-lath region shows brighter contrast in comparison to Figure 2a, suggesting a more pronounced enrichment of heavy elements (i.e., Ni) resulting from diffusional redistribution on aging and the potential formation of Ti_2Ni phase (compare Figure 3 in ref. [21]).

The microstructures formed by aging at 600 °C are closer to thermodynamic equilibrium than the quenched material conditions. The formation of the intermetallic phase is, hence, in better agreement with the thermodynamic predictions. Figure 2e,f, that is, the ternary alloys, shows similar contrast but substantial refinement in comparison to the binary alloy. Qualitatively, this observation agrees with the fact that both, Fe and Cr, are sluggishly diffusing and transforming elements.^[32,33] The hardness

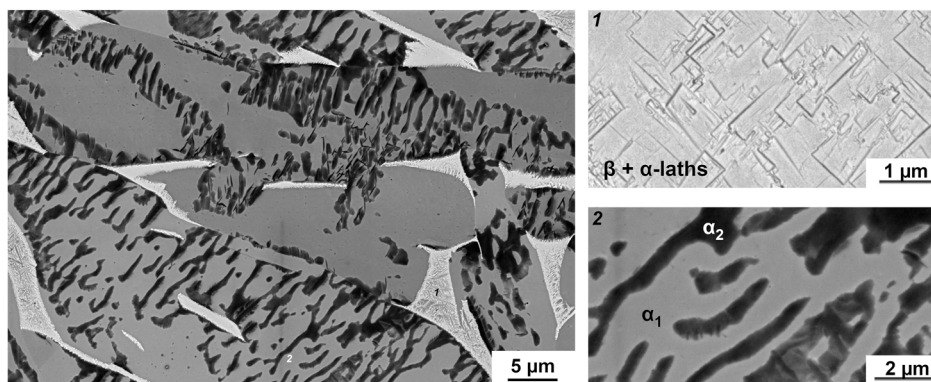


Figure 3. SEM BSE (5 kV, high noise-to-signal ratio [NSR] detector) image of the substructure formed in the Ti-6.4Ni alloy in condition 4. The insets highlight the microstructural constituents present, whereby the locations are labeled schematically (note that all alloys evidence this substructure in conditions 3 and 4).

values of these conditions, however, do not reflect hardening through the presence of the fine-scaled intermetallic phases as similar values are observed for all three alloys. Thus, it is suggested that the hardness is dominated by the α phase, which is depleted of alloying elements in this condition, resulting in reduced effects of solid-solution strengthening. This argumentation also explains the reduction in hardness in comparison to condition 1, where the formation of supersaturated α phase is likely the case.

Figure 2g–l shows the microstructural conditions resulting from direct aging for 1 h at 730 °C (condition 3, Figure 2g–i) and at 770 °C (condition 4, Figure 2j–l). These temperatures are around the eutectoid temperatures according to Figure 1. In these images, the β -stabilizing effect of Fe and Cr becomes prominently visible as the microstructures of the Fe- or Cr-modified alloys are much more dominated by this phase than the binary alloy. Fe and Cr are typically incorporated into the β phase in titanium alloys to a dominating extent. In a recent review by Prakash Kolli and Devaraj,^[34] it was suggested to use factors of 2.9 and 1.6 for the calculation of the molybdenum equivalent for Fe and Cr, respectively, thereby underpinning our argumentation with regard to the increasing amount of β phase and the β -stabilizing effect of these alloying elements.

Extremely fine substructures present within the β phase of all three alloys correspond to lath-like α phase, likely forming via a martensitic transformation.^[31,35,36] The α phase of all alloys in the direct aged material conditions evidences the presence of a substructure. Both will be treated in Subsection 2.3.

The hardness values evidence pronounced increases in hardness when comparing the ternary alloys to the binary one. This increase in hardness is considered to be an effect of the dominant β phase in these alloys, which has decomposed into a fine-scaled substructure strongly affecting the mean free path for dislocation motion (see Subsection 2.3 for more detailed discussion).

2.3. Structural Analysis and Phase Decomposition

The apparent phase decomposition of the α phase is shown in Figure 3. Here, the binary Ti-6.4Ni alloy in condition 4 has been

used exemplary but equivalent structures are visible in all alloys of conditions 3 and 4, that is, in the direct aged material conditions. In this figure, α - and β phases are visible, both evidencing a substructure with dimensions in the micrometer to nanometer range. In case of the β phase, this substructure corresponds to fine-scaled α -laths shown in detail in inset 1. The morphological appearance of these structures suggests that they could have formed via a martensitic transformation, which would be in agreement with available literature.^[31,35,36] In case of the α phase, clearly contrasted features are visible in Figure 3 and in the enlarged inset 2 (labeled with α_1 and α_2). The prevalent contrast in BSE mode suggests locally varying chemical compositions. Morphologically, the decomposition products appear in an aligned manner with meander-like characteristics. Such features have been reported often in association with spinodal decomposition products^[37–39]—a result of the soft impingement of the diffusional fields of solutes, dominating the morphological phase evolution during the transformations.

To further investigate the formation mechanism of the substructure in the interior of the α phase, XRD has been conducted for all three alloys. The corresponding diffraction patterns are shown in Figure 4a. Clearly, the major peaks are associated with the presence of α and β phases. Indications of small amounts of Ti_2Ni phase and β_0 phases are discernible. It should be mentioned that peak intensities may be affected by the textured nature of the button melts as well as peak broadening resulting from the fine dimension of such precipitates. The α -phase peaks show all evidence of splitting or at least the presence of a shoulder. In Figure 4b, one of the α -phase peaks is shown, which does not overlap with other peaks in the diffractogram. Its split shape is highlighted by dashed vertical lines. Using the peak positions from Figure 4b allows to calculate the differences in d-spacing observed here, which amounts to $\Delta d_{(10-12)} = 0.0017 \text{ \AA}$. The observed splitting is a further indication for spinodal decomposition (the underlying theory has been established by Daniel and Lipson^[40] and e.g., applied by Hernandez-Santiago et al.^[41] to underpin the prevalence of spinodal decomposition in the Cu-4wt%Ti system). Earlier work of Barriobero-Vila et al.^[35] on the Ti-6Al-6V-2Sn alloy has suggested that this mechanism can occur in titanium alloys, which was elucidated by the

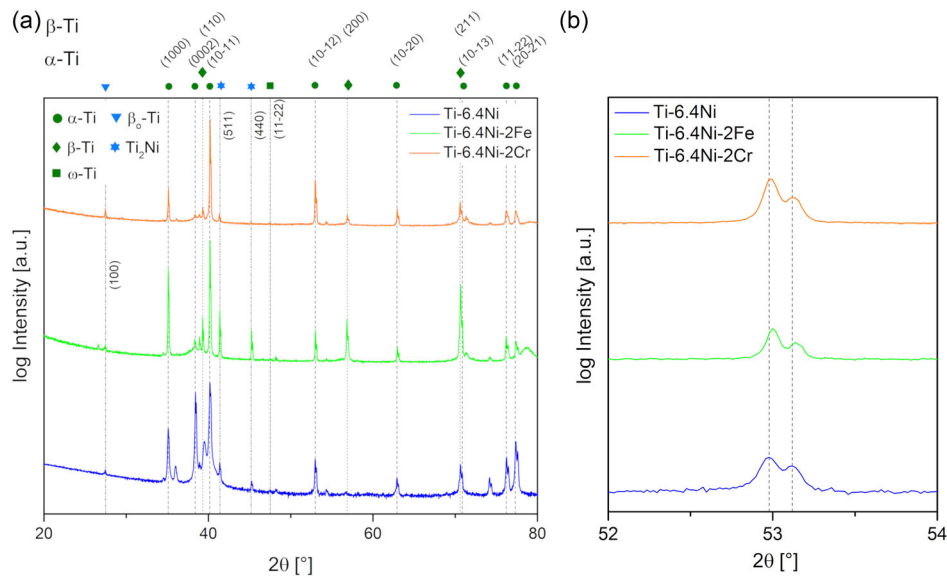


Figure 4. X-ray diffraction (XRD) diffractogram of all three alloys in condition 3, with a) indicated phases and b) highlighted region where α -phase peak splitting is clearly observed.

splitting of diffraction spots using transmission electron microscopy. The observed phenomenon appeared, however, on a very different length scale (of several nm) than in the present work.

In addition, Figure 4 shows the presence of peaks associated with the ω phase, whereby peaks are more pronounced in the ternary alloys. As the pronounced increase in hardness is a result of isothermal aging, the ω phase formed is argued to correspond to isothermal ω phase.^[42] The presence of isothermal ω phase can result in embrittlement, which would agree with the extremely high hardness values observed in the ternary alloys of the direct aged material conditions.^[43]

An exemplary EBSD inverse pole figure (IPF) map of the Ti–6.4Ni alloy in condition 4 is shown in Figure 5. The individual α grains are clearly visible. Poor indexing between the grains is a result of the phase mixture present in these regions (see Figure 3, inset 1). Within each grain, no indication of differing crystallographic features or varying orientations is observed. In combination with the results presented in Figure 4, the most likely cause of the contrasted features visible in Figure 3 is, therefore, suggested to be locally varying chemical variations.

2.4. Mechanical Properties

To determine the specific Young's moduli of the investigated alloys, their density was determined. This analysis resulted in values of $\rho_{\text{Ti6.4Ni}} = 4.61 \text{ g cm}^{-3}$, $\rho_{\text{Ti6.4Ni2Fe}} = 4.69 \text{ g cm}^{-3}$, and $\rho_{\text{Ti6.4Ni2Cr}} = 4.65 \text{ g cm}^{-3}$. Determination of the Young's modulus using ultrasound was conducted for the conditions 2 and 3. These conditions were chosen to assess the effect of the presence of intermetallic phases on the materials' specific stiffness. The resultant values are summarized in Table 1. The observed differences are comparably small, but a higher specific Young's modulus can be argued to be obtained in the presence of intermetallic

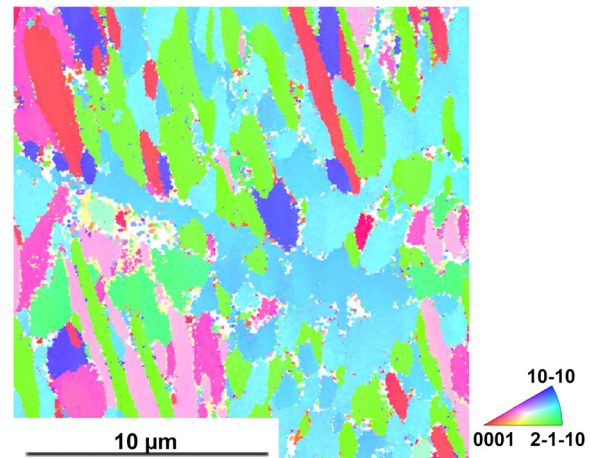


Figure 5. EBSD inverse pole figure (IPF) image of the Ti–6.4Ni alloy in condition 4. No evidence of differing crystallographic structure or differing orientations within each grain are observed.

Table 1. Values of the density-specific Young's modulus of the investigated alloys in material conditions 2 and 3.

	E/ρ of Ti–6.4Ni	E/ρ of Ti–6.4Ni–2Fe	E/ρ of Ti–6.4Ni–2Cr
Unit	[GPa (g cm ⁻³) ⁻¹]	[GPa (g cm ⁻³) ⁻¹]	[GPa (g cm ⁻³) ⁻¹]
Condition 2	26.0 ± 0.2	26.0 ± 0.4	26.0 ± 0.3
Condition 3	26.4 ± 0.3	25.1 ± 0.4	24.2 ± 0.4

phases, that is, condition 2. However, this effect overlaps with the differing α - and β -phase fractions and their differing elastic responses. The lower specific Young's modulus of the ternary alloys in condition 3 in comparison to the binary alloy may be

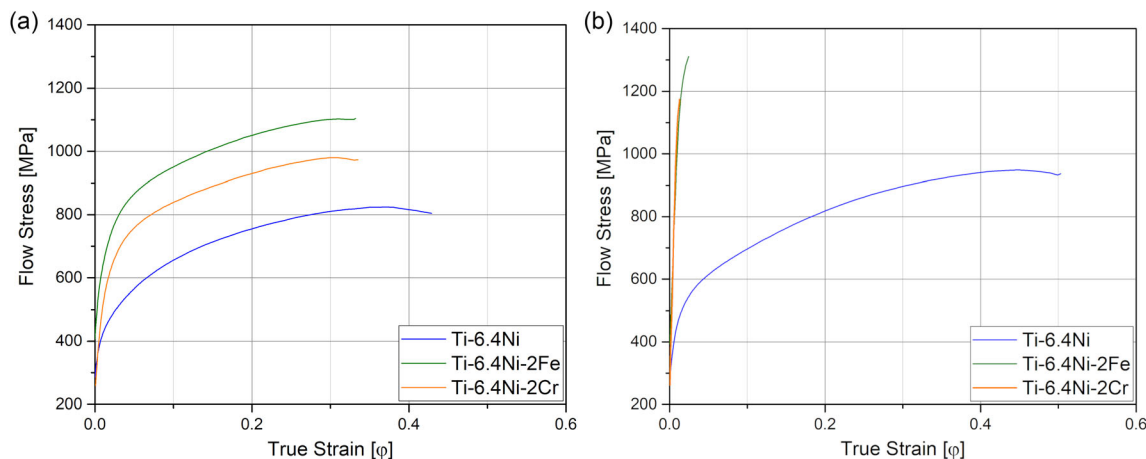


Figure 6. Room-temperature true stress–true strain compression curves of Ti alloys in a) condition 2 and b) condition 3 aged at 600 and 730 °C, respectively.

due to a high amount of β phase present in these material conditions as the β phase is known to have a lower Young's modulus than the α phase.^[44]

Compression testing curves of the equivalent material conditions are shown in **Figure 6**. Significantly higher strength values are observed through the ternary alloying element additions at the expense of ductility, with the addition of Fe having the strongest effect. The reduction of ductility is particularly pronounced in condition 3, which corresponds to the extremely high hardness of these samples (see **Figure 2**). In this condition, the phase fractions of the investigated alloys differ significantly, which suggests different behavior upon mechanical loading. During the extended aging procedure, isothermal ω phases may form, in agreement with our XRD results (**Figure 4**). These phases can result in embrittlement as has been shown in, for example, ref. [43]. Addition of Fe and/or Cr is therefore argued to be a suitable means to strengthen the Ti–6.4Ni alloy, provided that an appropriate heat-treatment procedure is followed.

3. Conclusion

The present work was undertaken to analyze the effects of ternary alloying element additions, namely Fe and Cr, on the eutectoid Ti–6.4Ni system. While Ni is an active eutectoid-forming element, Fe and Cr belong to the group of sluggish eutectoid-forming elements. The alloys were heat-treated to four different microstructural conditions and the resultant microstructures were characterized using SEM, XRD, hardness testing, Young's modulus determination, and compression testing. The following major conclusions can be drawn: 1) All three alloys form lath-like α phase upon rapid cooling with slightly different morphologies. During aging below the eutectoid temperatures, these lath-like α phases decompose allowing for Ti_2Ni intermetallic phase to form. 2) Direct aging without prior quenching does not result in the formation of a substantial amount of intermetallic Ti_2Ni phase. Instead, a substructure evolves within the α phase. Spinodal decomposition is identified as a possible cause based on its morphological appearance and

the occurrence of characteristic XRD peak splitting as well as the absence of differently orientated features in the EBSD. To the extent of our knowledge, the occurrence of this phenomenon has not been reported in the Ti–6.4Ni system so far. 3) The hardness of the quenched material conditions is governed by the characteristic lath dimensions; the hardness of the aged condition is governed by the alloying elements in solid solution; and the hardness of the direct aged conditions is governed by the presence of varying amounts of β phase and its decomposition products, including the effect of observed indications for the presence of ω phase. 4) The specific Young's modulus is slightly increased in the condition where the Ti_2Ni phase is present. The presence of ternary alloying element additions affects the Young's modulus as it affects the present fraction of phases. 5) The compression tests reveal lowest strength of the binary alloy and highest strength of the ternary alloy with Fe additions. The addition of alloying elements reduces the ductility to different extents depending on the heat treatment.

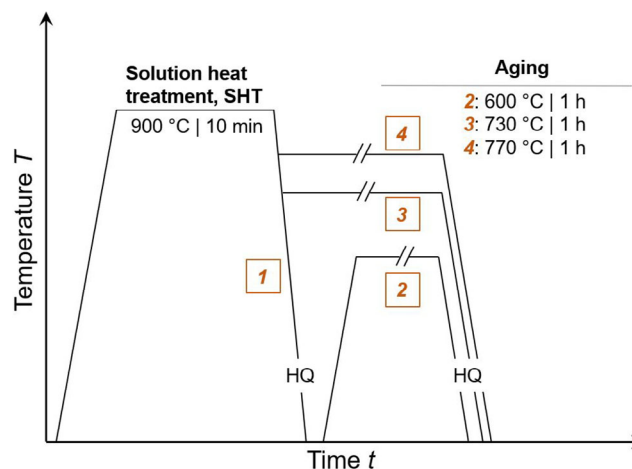


Figure 7. Scheme of the four different heat treatments performed in this study.

Table 2. Summary of conducted analyses and tests.

Alloy	Material condition	SEM	EBS	XRD	Hardness testing	Young's modulus determination	Compression testing
Ti–6.4Ni	Condition 1	×			×		
	Condition 2	×			×	×	×
	Condition 3	×		×	×	×	×
	Condition 4	×	×		×		
Ti–6.4Ni–2Fe	Condition 1	×			×		
	Condition 2	×			×	×	×
	Condition 3	×		×	×	×	×
	Condition 4	×			×		
Ti–6.4Ni–2Cr	Condition 1	×			×		
	Condition 2	×			×	×	×
	Condition 3	×		×	×	×	×
	Condition 4	×			×		

4. Experimental Section

Alloys and Processing Conditions: The alloys were fabricated into buttons of approximately 30 g using an arc melting system MAM-1 from Edmund Buehler GmbH. Buttons were melted and remelted three times to ensure chemical homogeneity. Arc-based button melting was used due to the process similarity with waDED (in terms of solidification conditions and cooling rate) and ease of use, whereby typical cooling rate values were in the range of approximately 50 °C s^{-1} .^[28,29] It was noted that the typical intrinsic heat treatment occurring during waDED processes could not be physically simulated by this procedure. The chosen chemical compositions were Ti–6.4Ni–(2.0X) in wt% whereby X corresponded to Fe and Cr. The molybdenum equivalents of these alloys were $\text{Mo}_{\text{eq,TiNi}} = 8.0$, $\text{Mo}_{\text{eq,TiNiFe}} = 13.8$, and $\text{Mo}_{\text{eq,TiNiCr}} = 11.2$ according to ref. [34].

Thermodynamic Calculations and Characterization Techniques: Phase fraction diagrams were calculated under equilibrium conditions using Thermo–Calc 2021b with the TCTi3 thermodynamic database.

Heat treatments were conducted using a Bähr DIL 805 A/D dilatometer under atmospheric conditions and quenched using helium gas quenched. Subsequently, three types of aging treatments were conducted as visualized schematically in **Figure 7**. It was pointed out that conditions 3 and 4 were generated by annealing without prior quenching to ambient temperature, referred to as direct aging.

A summary of all conducted analyses and tests is given in **Table 2**. Microstructure characterization by SEM was conducted on all materials after the heat treatment. Preparation was performed using successively finer abrasive paper grades with final mechanochemical polishing with colloidal silica. Characterization was conducted in an Tescan Mira 3 SEM equipped with a four-quadrant solid-state backscattered electron (BSE) detector (4Q-BSE), operated at 15 kV acceleration voltage. High-resolution BSE images were taken with a Gatan high noise-to-signal ratio (NSR) detector at 5 kV acceleration voltage. EBSD was performed using an EDAX Velocity Super EBSD camera 4500 pps at a working distance of 20 mm. Data evaluation was carried out using the EDAX OIM software. α and β titanium phases were included for indexing (only α -Ti shown here). The dataset underwent a grain boundary dilation cleanup with a tolerance angle of 5° and the minimum grain size was set to 10 pixels. Moreover, a neighbor confidence index correlation with a minimum confidence index of 0.1 was used.

XRD was performed on a Siemens X'pert powder diffractometer in Bragg–Brentano geometry with X'Celerator detectors. $\text{Cu-K}\alpha$ radiation was applied. The scans were conducted with steps of 0.02° . Phase analysis was performed with the X'pert HighScore software.

Hardness determination was carried out using a DuraScan 70 G5 microhardness tester (EMCO-TEST) from ZwickRoell GmbH & Co KG with 100 g load. Each material condition was tested with at least eight indents and the reported values corresponded to their mean.

For the determination of the specific Young's moduli, the densities of the alloys were determined using Archimedes' principle. The Young's moduli were determined by nine individual measurements at 15 MHz with the Phasor XS phased array ultrasound device from GE Inspection Technologies. The CLF-4 probe was used for longitudinal oscillation and the K7/KY probe was used for transversal oscillation.

Compression testing was carried out with a servo hydraulic thermomechanical treatment simulator from Servotest Testing Systems Ltd. Tests were conducted at ambient temperature at a deformation rate of 0.1 s^{-1} , up to a degree of deformation of 0.7. For compression testing, cylindrical specimens of 8 mm diameter and 12 mm in length were machined from the alloy buttons.

Acknowledgements

This research has been funded by the Austrian Federal Ministry for Climate Action, Environment, Energy, Mobility, Innovation and Technology (BMK) within the “Austrian Space Applications Program, ASAP” in the project “Ti4Space – Optimized Titanium Alloys for Space Applications Processed by Directed Energy Deposition” (grant agreement no. 885338) administered by FFG. Fruitful discussions with Prof. M. Stockinger (Chair of Metal Forming, Montanuniversität Leoben) and experimental assistance by T. Teeuwen (Institute of Metal Forming, RWTH Aachen University) are greatly appreciated.

Conflict of Interest

The authors declare no conflict of interest.

Data Availability Statement

The data underlying this study cannot be shared at the moment as it forms part of an ongoing study.

Keywords

eutectoid transformation, mechanical properties, microstructure characterization, phase transformations, titanium alloys

Received: February 7, 2023

Revised: April 28, 2023

Published online:

- [1] F. H. Froes, *Titanium: Physical Metallurgy, Processing and Applications*, ASM International, Materials Park, OH **2015**.
- [2] C. R. Cunningham, S. Wikshåland, F. Xu, N. Kemakolam, A. Shokrani, V. Dhokia, S. T. Newman, *Procedia Manuf.* **2017**, *11*, 650.
- [3] D. Herzog, V. Seyda, E. Wycisk, C. Emmelmann, *Acta Mater.* **2016**, *117*, 371.
- [4] T. Lehmann, D. Rose, E. Ranjbar, M. Gasri-Khouzani, M. Tavakoli, H. Henein, T. Wolfe, A. J. Qureshi, *Int. Mater. Rev.* **2022**, *67*, 410.
- [5] K. Treutler, V. Wesling, *Appl. Sci.* **2021**, *11*, 8619.
- [6] B. Wu, Z. Pan, D. Ding, D. Cuiuri, H. Li, J. Xu, J. Norrish, *J. Manuf. Process.* **2018**, *35*, 127.
- [7] G. Venturini, F. Montevecchi, F. Bandini, A. Scippa, G. Campatelli, *Addit. Manuf.* **2018**, *22*, 643.
- [8] F. Michel, H. Lockett, J. Ding, F. Martina, G. Marinelli, S. Williams, *Rob. Comput. Integr. Manuf.* **2019**, *60*, 1.
- [9] H. Lockett, J. Ding, S. Williams, F. Martina, *J. Eng. Des.* **2017**, *28*, 568.
- [10] M. Gudeljevic, T. Klein, *Int. J. Adv. Manuf. Technol.* **2021**, *116*, 2021.
- [11] F. H. S. Froes, M. N. Gungor, M. A. Imam, *JOM* **2007**, *59*, 28.
- [12] I. Gibson, D. Rosen, B. Stucker, M. Khorasani, *Additive Manufacturing Technologies*, Springer, Cham, Switzerland **2021**.
- [13] A. A. Antony, J. Meyer, P. B. Prangnell, *Mater. Charact.* **2013**, *84*, 153.
- [14] B. E. Carroll, T. A. Palmer, A. M. Beese, *Acta Mater.* **2015**, *87*, 309.
- [15] M. Neikter, R. Woracek, T. Maimaitiyili, C. Scheffzük, M. Strobl, M. L. Antti, P. Åkerfeldt, R. Pederson, C. Bjerkén, *Addit. Manuf.* **2018**, *23*, 225.
- [16] D. Zhang, D. Qiu, M. A. Gibson, Y. Zheng, H. L. Fraser, D. H. StJohn, M. A. Easton, *Nature* **2019**, *576*, 91.
- [17] M. Simonelli, D. G. McCartney, P. Barriobero-Vila, N. T. Aboulkhair, Y. Y. Tse, A. Clare, R. Hague, *Metall. Mater. Trans. A* **2020**, *51*, 2444.
- [18] T. Klein, M. J. Paul, C. Simson, J. Niedermayer, B. Gludovatz, *Mater. Lett.* **2022**, *319*, 132305.
- [19] B. A. Welk, N. Taylor, Z. Kloenne, K. J. Chaput, S. Fox, H. L. Fraser, *Metall. Mater. Trans. A* **2021**, *52*, 5367.
- [20] M. Chen, S. Van Petegem, Z. Zou, M. Simonelli, Y. Y. Tse, C. S. T. Chang, M. G. Makowska, D. Ferreira Sanchez, H. Moens-Van Swygenhoven, *Addit. Manuf.* **2022**, *59*, 103173.
- [21] P. L. Narayana, J. H. Kim, S. Lee, J. W. Won, C. H. Park, J. T. Yeom, N. S. Reddy, J. K. Hong, *Scr. Mater.* **2021**, *200*, 113918.
- [22] Z. Xiong, X. Pang, S. Liu, Z. Li, R. D. K. Misra, *Scr. Mater.* **2021**, *195*, 113727.
- [23] G. Choi, W. S. Choi, J. Han, P. P. Choi, *Addit. Manuf.* **2020**, *36*, 101467.
- [24] A. V. Dobromyslov, *Phys. Met. Metallogr.* **2021**, *122*, 237.
- [25] H. J. Lee, H. I. Aaronson, *J. Mater. Sci.* **1988**, *23*, 150.
- [26] T. A. Bhaskaran, R. V. Krishnan, S. Ranganathan, *Metall. Mater. Trans. A* **1995**, *26*, 1367.
- [27] H. Wang, N. Warnken, R. C. Reed, *Calphad* **2011**, *35*, 204.
- [28] A. Ho, H. Zhao, J. W. Fellowes, F. Martina, A. E. Davis, P. B. Prangnell, *Acta Mater.* **2019**, *166*, 306.
- [29] Z. Zhiyi, M. Simonelli, A. Clare, N. Aboulkhair, R. Hague, in *Alloy. Addit. Manuf. Symp.*, Munich **2022**.
- [30] T. Klein, G. Graf, P. Staron, A. Stark, H. Clemens, P. Spoerk-Erdely, *Mater. Lett.* **2021**, *303*, 130500.
- [31] S. L. Semiatin, T. R. Bieler, *Acta Mater.* **2001**, *49*, 3565.
- [32] H. Nakajima, M. Koiwa, *ISIJ Int.* **1991**, *31*, 757.
- [33] P. G. Esteban, E. M. Ruiz-Navas, E. Gordo, *Mater. Sci. Eng. A* **2010**, *527*, 5664.
- [34] R. P. Kolli, A. Devaraj, *Metals* **2018**, *8*, 506.
- [35] P. Barriobero-Vila, V. Biancardi Oliveira, S. Schwarz, T. Buslaps, G. Requena, *Acta Mater.* **2017**, *135*, 132.
- [36] H. Nakashima, J. Yu, M. Takeyama, *Calphad* **2023**, *80*, 102521.
- [37] V. Sofonea, K. R. Mecke, *Eur. Phys. J. B* **1999**, *8*, 99.
- [38] E. O. Avila-Davila, D. V. Melo-Maximo, V. M. Lopez-Hirata, O. Soriano-Vargas, M. L. Saucedo-Muñoz, J. L. Gonzalez-Velazquez, *Mater. Charact.* **2009**, *60*, 560.
- [39] J. Zhu, L. Q. Chen, J. Shen, V. Tikare, *Phys. Rev. E* **1999**, *60*, 3564.
- [40] V. Daniel, H. Lipson, *Proc. R. Soc. London. Ser. A* **1943**, *181*, 368.
- [41] F. Hernandez-Santiago, N. Cayetano-Castro, V. M. Lopez-Hirata, H. J. Dorantes-Rosales, J. De Jesus Cruz-Rivera, *Mater. Trans.* **2004**, *45*, 2312.
- [42] A. X. Y. Guo, C. Geng, Z. Lin, *J. Mater. Sci. Eng.* **2022**, *11*.
- [43] M. J. Lai, T. Li, F. K. Yan, J. S. Li, D. Raabe, *Scr. Mater.* **2021**, *193*, 38.
- [44] A. Nocivin, D. Raducanu, B. Vasile, C. Trisca-rusu, E. M. Cojocar, A. Dan, R. Irimescu, V. D. Cojocar, *Materials* **2021**, *14*, 3467.